THE JOURNAL OF PHYSICAL CHEMISTRY B

Article

pubs.acs.org/JPCB

Excited-State Proton Transfer of Photoacids Adsorbed on Biomaterials

Nadav Amdursky,[†] Ron Simkovitch,[‡] and Dan Huppert*[,‡]

[†]Department of Materials, Imperial College London, London SW7 2AZ, United Kingdom

[‡]Raymond and Beverly Sackler Faculty of Exact Sciences, School of Chemistry, Tel Aviv University, Tel Aviv 69978, Israel

Supporting Information

ABSTRACT: The interaction between a photoacid (8-hydroxy-1,3,6-pyrenetrisulfonate, HPTS) and the surfaces of biomaterials and the diffusion of protons along the biomaterial surfaces were examined by following the excited-state proton transfer (ESPT) from the photoacid, adsorbed on the surfaces, to water molecules next to it. We chose two different types of biomaterial surfaces, hydrophobic insulin amyloid fibrils and hydrophilic cellulose surfaces. With the help of steady-state and time-resolved fluorescence techniques, we found that the rate of ESPT from HPTS on insulin fibrils to adjacent water molecules is about $^1/_{10}$ that in bulk water. However, the proton geminate recombination takes place with an efficiency similar to that in bulk water. ESPT from HPTS in wet cellulose to water depends on the weight percentage of water adsorbed by the cellulose. In a semidry sample (<100% weight percentage of water), the ESPT rate is rather low and thus the quantum efficiency of the ESPT is also low within the excited-state lifetime. When the water content is higher, the ESPT rate is almost that of bulk water. We explain these results by the existence of pools of water in cellulose of high water content, in which the triple-negatively charged HPTS molecules desorb from the cellulose surface to these pools. The use of HPTS has allowed us to examine the biological surface and its interaction with water molecules, while obtaining important information regarding the hydration state of the surface that otherwise could not have been obtained. The model that we propose here for the use of photoacids to follow the hydrated state of a given surface is a promising new method of examining the interaction of water molecules with biological surfaces.

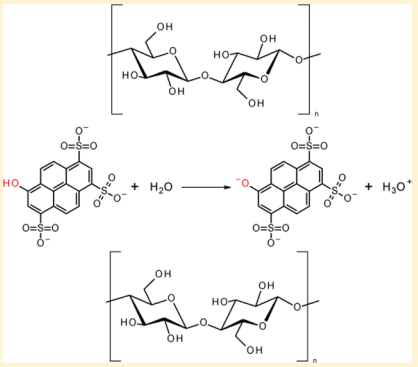

INTRODUCTION

Much scientific effort has been employed to understand the interaction of small molecules with biological surfaces. In general, while excluding the interactions between binding sites to specific molecules, small molecules can be either attracted to the biological surface (mainly by electrostatic or hydrophobic forces) or remain hydrated even in close proximity to the surface. Much of the biological processes involve the reaction of water molecules or protons/hydronium ions (such as hydrolysis, phosphorylation, ionic conduction, proton-coupled electron transfer, and many more), thus understanding the proton transfer along biological surfaces and their corresponding hydration layer is of prime importance. In this work, we propose a model for the use of photoacids in order to get new insights on the latter points. In order to examine the validity of the model, we explore the interaction of the 8-hydroxypyrene-1,3,6-trisulfonate (HPTS) photoacid with two highly different biological surfaces; the first one is amyloid fibrils, and the second is a cellulose matrix.

The formation of amyloid fibrils involves the aggregation of the soluble amyloid protein into an insoluble structure of amyloid fibrils. This structure of amyloid fibrils and its interaction with small molecules has been studied extensively,[1−7] mainly with the purpose of finding inhibitors for the formation of the amyloid fibrils that are associated with several neurodegenerative diseases (such as Alzheimer's, Parkinson's, type II diabetes, and more). The consensus of the latter studies is that the fibrils are composed of a cross-β structure (Figure 1a), in which the β-sheets are in contact with one another by their side groups. In this way, molecules can bind to amyloid fibrils via electrostatic charges (to negative or positive grooves, red and blue regions, respectively, in Figure 1b) or to hydrophobic grooves (white regions in Figure 1b) along the cross-β structure. For example, one of the most studied interactions between small molecules and amyloid fibrils is that between the fibrils and the thioflavin T (ThT) dye, which is commonly used for the detection of amyloid fibrils.[8] In this context, it was hypothesized that ThT binds perpendicular to the β-sheet striation in one of the hydrophobic grooves along the fibril structure,[9,10] which in turn inhibits its intramolecular rotation and increases its fluorescence intensity.[11]

Cellulose is a polysaccharide $(C_6H_{10}O_5)_n$ consisting of a long linear chain with several hundred to over ten thousand linked D-glucose units (Figure 2a), which can be found in the cell walls of green plants.[12,13] Accordingly, it is the most abundant organic polymer on Earth.[14] Cellulose consists of D-glucose

Received: September 10, 2014
Revised: October 19, 2014
Published: November 7, 2014

dx.doi.org/10.1021/jp509153r | J. Phys. Chem. B 2014, 118, 13859−13869

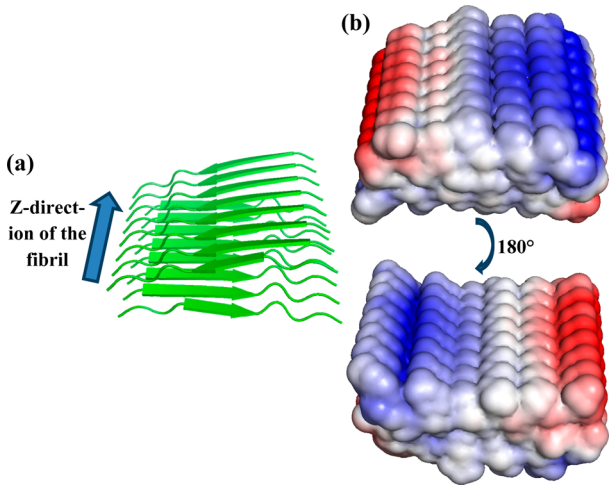

Figure 1. (a) The cross-β structure of amyloid fibrils. PDB ID: 2M5N. (b) An electrostatic surface sphere preview of part a showing the charged and hydrophobic grooves along the cross-β structure. The red and blue colors represent negative and positive electrostatic charges, respectively.

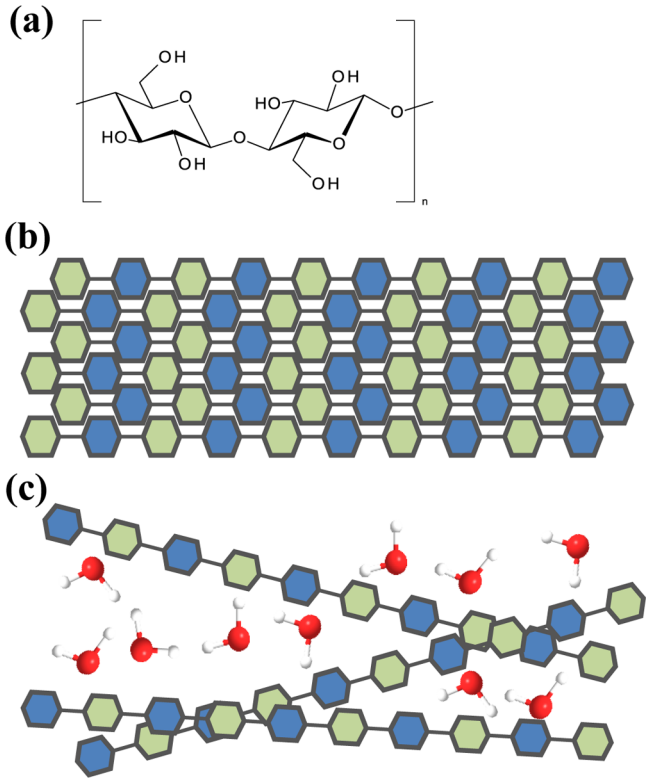

Figure 2. (a) Molecular structure of cellulose and a schematic representation of the molecular packing in (b) the dry (crystalline) and (c) hydrated states.

units that condense through $\beta(1\rightarrow4)$-glycosidic bonds. In starch, the linkage between the D-glucose units is based on $\alpha(1\rightarrow4)$-glycosidic bonds. Unlike starch, cellulose is a straight-chain polymer with no coiling or branching. Many properties of cellulose depend on its chain length or degree of polymerization. Cellulose from wood pulp has typical chain lengths of between 300 and 1700 units. It has both crystalline and amorphous regions, and upon hydration, it can absorb water molecules at a ratio of nearly 5:1 (H_2O:cellulose),[15] thus creating a matrix that might resemble the structure of hydrogels (parts b and c of Figure 2 show a representation of dry and hydrated cellulose). Microcrystalline cellulose has been referred to as a "molecular sponge" by Fielden et al.[16] because most of the water held by cellulose is present as free water that may be readily lost by evaporation.

Here we explore not only the binding of small molecules to biological surfaces but also how they interact with the structure of the surface and the water molecules surrounding it. For this purpose, we have used HPTS (shown in Scheme 1), which has a hydrophobic part (pyrene), a polar group (hydroxyl), and charged groups (sulfonate).

Scheme 1. Molecular Scheme of HPTS

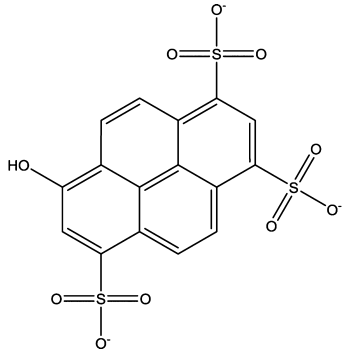

HPTS is a photoacid, which means that it has different pK_a values in its ground and excited states, 7.4 and 1.3, respectively (a striking difference of 6 orders of magnitude in the K_a values). Upon excitation (see the full photoprotolytic cycle in Scheme 2), the excited-state acid, ROH*, can exhibit an intermolecular

Scheme 2. Photoprotolytic Cycle of Photoacids[a]

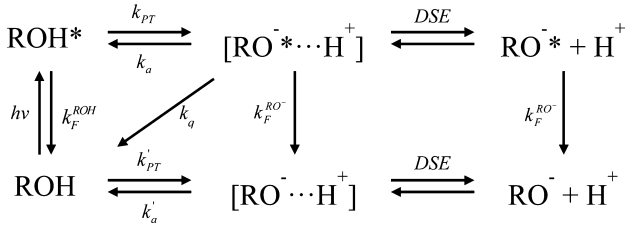

[a]DSE stands for Debye–Smoluchowski equation (see text).

proton transfer (k_{PT}) from the acid group to nearby solvent molecules to form an ion pair, $RO^{-}{}^{*}\cdots H^{+}$. We refer to this process here as an excited-state proton transfer (ESPT) process.

Following the ESPT process, the proton in the ion pair can either diffuse to the bulk solvent, $RO^{-}{}^{*} + H^{+}$, which can be described by the Debye–Smoluchowski equation (DSE),[17,18] or recombine with the excited deprotonated state, $RO^{-}{}^{*}$, to return to the ROH* state by what is known as the geminate recombination process. Since the ROH* and $RO^{-}{}^{*}$ states have different emission peak positions (~440 and 512 nm, respectively), it is relatively easy to follow each of the species by time-resolved fluorescence in order to follow the proton diffusion.

Thus, with a knowledge of the proton diffusion constant in water ($\sim 9 \times 10^{-5}$ cm^2/s), one can calculate the distance (in three dimensions) that the proton can travel within the excited-

dx.doi.org/10.1021/jp509153r | J. Phys. Chem. B 2014, 118, 13859–13869

state lifetime of HPTS (~5 ns). This can reach a distance of ~150 Å. In this way, HPTS has been used to calculate the distance of confined aqueous volumes within structures, such as reverse micelles[19,20] or within hydrogels.[21] In close proximity to surfaces, the photoexcited proton-transfer rate from HPTS to a water molecule can be affected by the presence of the surface. In this context, it has been shown that the diffusion space of protons released from HPTS next to surfaces of oxidized porous silicon[22] or alumina[23] is more two-dimensional than the common three-dimensional diffusion space in bulk solution (further explained in the Theoretical Model section). In the present study, we follow the time-resolved and steady-state fluorescence of HPTS in the presence of amyloid fibrils and cellulose matrix, in order to obtain insight on the hydration state of these biomaterial surfaces. Specifically, we will determine if (and how) HPTS can be adsorbed on the surface of the biological material, how the released protons diffuse along the surface, and whether any small confined aqueous volumes can be formed adjacent to the surface.

MATERIALS AND METHODS

8-Hydroxypyrene-1,3,6-trisulfonate (HPTS), recombinant human insulin, and cellulose 20 μm powder were purchased from Sigma-Aldrich.

The insulin fibrils were formed by dissolving the recombinant human insulin powder in a solution of 100 mM NaCl (pH 1.6) at a final insulin concentration of 2 mg/mL, followed by heating the sample at 65 °C for ~4 h without mechanical agitation. In order to change the buffer conditions, the solution of insulin fibrils formed was centrifuged at 10 000 rpm for 5 min, and the supernatant was replaced with water at pH 6.6.

Measurements of time-correlated single-photon counting (TCSPC) were performed with the use of excitation from a cavity-dumped titanium:sapphire femtosecond laser (Mira, Coherent), which provides short, 150 fs pulses at approximately 800 nm. The second harmonic of the laser, operating over the spectral range of 380−420 nm, was used to excite the samples. The cavity dumper operated with a relatively low repetition rate of 800 kHz. The TCSPC detection system was based on a Hamamatsu 3809U photomultiplier and an Edinburgh Instruments TCC 900 computer module for TCSPC. The overall instrument response was approximately 40 ps (full width at half-maximum, fwhm) where the excitation pulse energy was reduced to about 10 pJ by neutral-density filters.

The steady-state emission and absorption spectra were recorded by a Horiba Jobin Yvon FluoroMax-3 spectrofluorimeter.

THEORETICAL MODEL

The ESPT Geminate-Recombination Model. Scheme 2 shows a model that describes the photoprotolytic cycle of a photoacid.[24,25] The model accounts not only for the step of proton transfer to the solvent but also for the probability that the proton recombines with the excited-state deprotonated molecule to reform an excited-state photoacid. The proton-geminate-recombination step is seen as a nonexponential long-time fluorescence tail that obeys a power-law decay of $t^{-\alpha}$. The decay law is sensitive to the proton-diffusion-space dimension. As we will show later, this diffusion space is not three-dimensional in the complex structures that we study in this work.

Reversible and Irreversible Photoprotolytic Cycles of Photoacids. Excitation of a photoacid solution at a pH lower than its ground-state pK_a generates a vibrationally relaxed, electronically excited ROH molecule (denoted by ROH*) that initiates a photoprotolytic cycle (Scheme 2). Proton dissociation, with an intrinsic rate constant, k_{PT}, leads to the formation of an ion-pair $RO^-{}^*\cdots H^+$ which subsequently forms an unpaired $RO^-{}^*$ and a solvated proton, that diffuses into the bulk of the solution. The proton and $RO^-{}^*$ may recombine via reversible (adiabatic) recombination with a rate constant, k_a, and reform the excited acid, ROH*. In general, back-protonation may also proceed by an irreversible (nonadiabatic) pathway, involving fluorescence quenching of the $RO^-{}^*$ by a proton with a rate constant, k_q, forming the ground-state ROH.

Removal of an ion-pair from the contact radius, a, to infinity is described by the transient numerical solution of the Debye−Smoluchowski equation (DSE).[17,26] The motion of the transferred proton in water near the photoacid depends strongly on the electrical potential existing between it and the deprotonated form. The diffusion-assisted geminate recombination of $RO^-{}^*$ with the proton can be quantitatively described with the use of a numerical solution of the DSE under the initial and boundary conditions of the photoprotolytic process. In addition, the fluorescence lifetimes of all excited species are considered, with $1/k_F^{ROH} = \tau_{ROH}$ for the acid and $1/k_F^{RO^-} = \tau_{RO^-}$ for the conjugate base. Generally, $k_F^{RO^-}$ and k_F^{ROH} are much smaller than both the proton-reaction and the diffusion-controlled rate constants. The amplitude of the long-time fluorescence tail of ROH* depends on the intrinsic rate constants, k_a and k_{PT}, on the proton-diffusion coefficient, D_{H^+}, and on the electrical potential between $RO^-{}^*$ and the proton.

Time-Resolved Fluorescence-Data Analysis with the Use of the Geminate-Recombination Model. HPTS is a negatively charged, reversible, mild photoacid with $pK_{a,chem}^* \approx 0.7$ ($pK_{a,chem}^* = pK_a^* - \Delta pK_{a,elec}^* = 1.3-0.6$). One must differentiate between the pK_a value and the p$K_{a,chem}$ value. The difference arises from the thermodynamic definition of ΔG for the acid dissociation reaction. The ΔG of the acid dissociation reaction is defined as the removal of a proton far away from the RO^- anion. The Coulomb attraction between the proton and the RO^- has to be overcome in order to remove the proton from the contact radius a to "infinity". The free energy cost of the proton removal is called ΔG_{elec} and results in the difference between the pK_a value and the p$K_{a,chem}$ value. For HPTS with a negative charge of 4 e^-, the difference is about 0.7 pK units. Mild photoacids with $pK_{a,chem}^* > 0$ transfer a proton within the excited-state lifetime to H_2O but not to alcohols like methanol and ethanol and other protic liquids. It is estimated that the ESPT rate constant, k_{PT}, of HPTS to methanol is about 4 orders of magnitude smaller than that in H_2O. In H_2O, $k_{PT} \approx 10^{10}$ s^{-1} ($\tau_{PT} \approx 100$ ps) and thus the ESPT rate for methanol is about $\sim 10^6$ s^{-1}, smaller by a factor of 200 than the radiative rate $k_F \sim 2 \times 10^8$ s^{-1}. The ESPT rate of mild photoacids (i.e., with $pK_a^* > 0$) is very sensitive, not only to the protic solvent but also to the state of water. Strongly bound water, for example, does not participate in the ESPT process,[27] and as we will discuss later, water that is bound to fibrils or cellulose might not be a good proton acceptor.

HPTS RO^- has four negative charges, and the Coulomb attraction $RO^-{}^*\cdots H^+$ is very high. HPTS therefore serves as an example for the geminate-recombination model, since the relative tail intensity of ROH fluorescence is very high and is

dx.doi.org/10.1021/jp509153r | J. Phys. Chem. B 2014, 118, 13859−13869

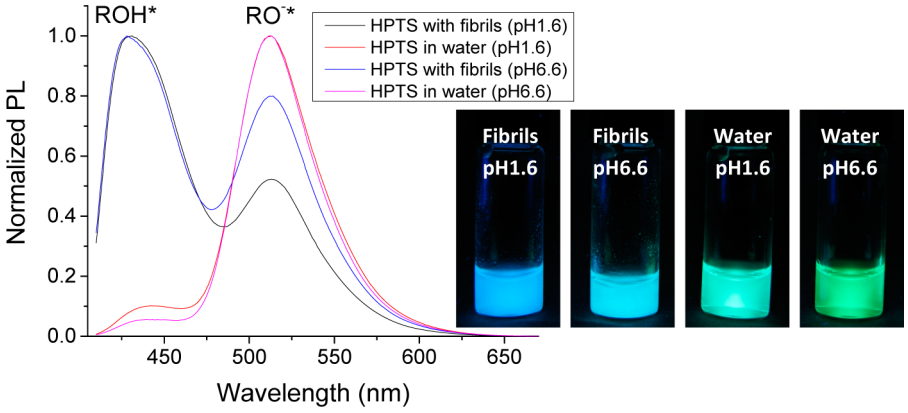

Figure 3. Steady-state emission spectrum of HPTS in bulk water and in the presence of insulin fibrils at pH 1.6 and at pH 6.6. The images show the emission of the solutions upon excitation over the range 360−390 nm.

easily measured, even at long times of about 20 ns, 4 times longer than the fluorescence decay time of both the ROH and RO^- forms. The long-time tail of the fluorescence, when compensated by multiplying the signal by $\exp[t/\tau_F]$ for the finite excited-state lifetime, decays according to a power law - $t^{-\alpha}$. The asymptotic long-time expression for the amplitude and the decay law is given by

$$I_f^{ROH}(t) \sim \frac{\pi a^2 k_a \exp[-V(a)]}{2k_{PT}(\pi D)^{d/2}} t^{-d/2} \quad (1)$$

where a is the reaction-sphere radius, k_{PT} and k_a are the intrinsic ESPT and geminate recombination rates occurring on the reaction sphere, $-V(a)$ $(=R_D/a)$ is the potential at the reaction sphere, D is the mutual diffusion coefficient between RO^- and H^+, and d is the diffusion-space dimension. R_D, the Debye radius, is given by

$$R_D = \frac{|z|e^2}{\varepsilon k_B T}$$

where z is the RO^- form charge, in electron charge units, e is the electron charge, and ε is the dielectric constant of the medium. This expression predicts a nonexponential fluorescence decay that fits a power law of $t^{-d/2}$. Equation 1 indicates that the amplitude of the long fluorescence depends on many parameters, but the decay law depends only on the dimension of the diffusion space.

In the past, we used the program of Krissinel and Agmon[28] for solving the spherically symmetric diffusion problem (SSDP) that was designed to solve the problem of geminate recombination. This was done in order to fit the time-resolved emission signals of HPTS and other photoacids in a confined volume of bulk water. The parameters that govern the time-resolved emission of the ROH or RO^- signals are the ESPT rate constant and the intrinsic rate of geminate recombination, k_{PT} and k_a, respectively. k_{PT} controls the initial ROH signal decay, and thus, it can be determined with minimum interference from all the other parameters (D, a, d, R_D, k_F^{ROH}, and $k_F^{RO^-}$) (see Scheme 2), which control the amplitude and shape of the intermediate and long-time decays.[24,25] The proton diffusion constant for bulk water is 9×10^{-5} cm^2/s. We used this value for H_2O samples and the value of 6×10^{-5} cm^2/s for the D_2O samples. For the reaction-sphere radius, a, we used a = 6 Å. The diffusion-space dimension, d, is used as an adjustable parameter. As we will show later, while for bulk water and D_2O the diffusion-space dimension is d = 3, it differs when HPTS is adsorbed on either insulin fibrils or cellulose. The Coulomb attraction potential is defined by R_D, and for the dielectric constant of water, ε_{H_2O}, and HPTS RO^- charge of $-4e$, we obtain R_D = 28 Å. This means that, at 28 Å, the Coulomb potential and the thermal energy k_BT are equal, where T is room temperature. As seen in eq 1, R_D has an exponential effect on the amplitude of the ROH nonexponential fluorescence tail.

The excited-state radiative lifetimes for both the ROH and RO^- forms of HPTS are similar, at $\tau_F \approx 5.4$ ns. The excited-state populations of both ROH and RO^- decrease exponentially. The intensity of the time-resolved emission signals at long times, of both the ROH and RO^- forms, is determined by the radiative rate. In bulk water and D_2O, the ROH fluorescence of HPTS is considered a textbook example of the reversible diffusion-assisted proton geminate recombination model.[24,25] The ROH signal in water and D_2O can be fitted in almost perfect agreement with the model, to about 4 orders of magnitude of intensity and within a wide time window of 0−20 ns extended to about four lifetimes. The parameters of bulk water are $k_{PT} = 10^{10}$ s^{-1}, k_a = 7.3 Å/ns, $D = 9 \times 10^{-5}$ cm^2/s, d = 3, a_0 = 6 Å, and τ_f = 5.4 ns. The value of τ_F^{ROH} is obtained by exciting HPTS in ethanol, and that of $\tau_F^{RO^-}$ either by the long-time slope of the TCSPC signal measured at $\lambda \geq 520$ nm or by direct excitation of the RO^- form of HPTS in a basic solution.

RESULTS

HPTS on Insulin Fibrils. The k_{PT} of HPTS in aqueous solution is $\sim 10^{10}$ s^{-1}. Thus, upon excitation, the dominant species at times t > 100 ps is RO^-*, rather than ROH*. Consequently, the steady-state emission spectrum of HPTS in bulk water (under not very acidic conditions) exhibits mainly the band around 512 nm (magenta curve, Figure 3). Upon lowering of the pH to 1.6, the working buffer for the formation of the fibrils (see the Materials and Methods), the percentage of the ROH* increases slightly (red curve, Figure 3), but the RO^-* population is still predominant. However, in the presence of insulin fibrils, the population distribution is completely reversed, with ROH* predominant at both pH 1.6 and 6.6. The reversal of the populations can be the result of two possibilities or, most probably, a combination of them: (1) The rate of proton transfer (k_{PT}) from HPTS to the bulk water upon excitation is smaller when the molecules are adsorbed on the fibrils than when they are in bulk water. (2) The geminate

dx.doi.org/10.1021/jp509153r | J. Phys. Chem. B 2014, 118, 13859−13869

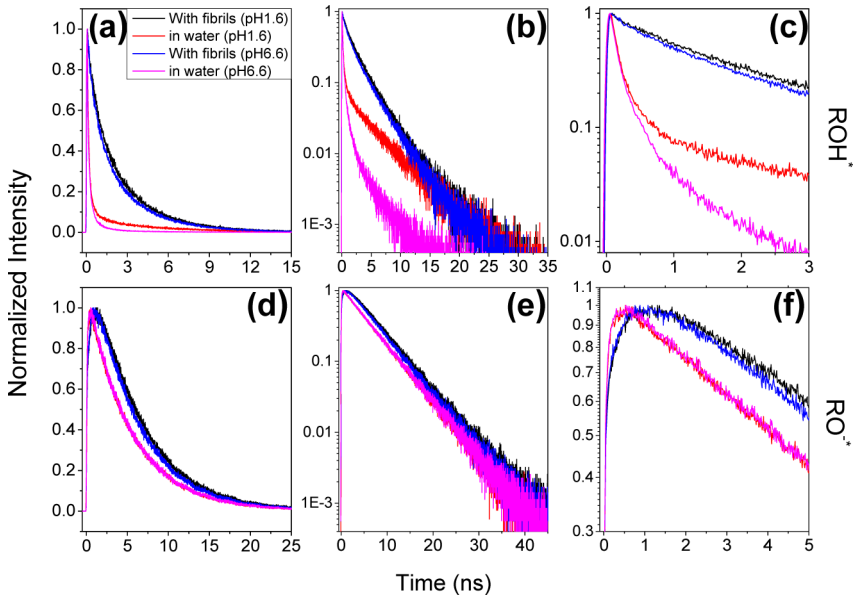

Figure 4. Time-resolved emission of HPTS adsorbed on insulin fibrils at the detection wavelength of ROH* (440 nm) and RO^-* (535 nm), top and bottom graphs, respectively, in the presence of insulin fibrils (black and blue curves for buffers of pH 1.6 and 6.6, respectively) and in bulk water (red and magenta curves for buffers of pH 1.6 and 6.6, respectively). Parts a and d are on a linear scale, parts b and e are on a semilogarithmic scale, and parts c and f are magnifications of parts b and e, respectively.

recombination process (k_a) is highly efficient when HPTS is adsorbed on the fibrils.

In order to determine which of the latter possibilities is the main one, and also to follow directly the dynamics of the process, we turned to studies of time-resolved emission. Figure 4 shows the time-resolved emission of HPTS at the detection wavelengths of ROH* and RO^-*, in the upper and lower graphs, respectively (Figure S1, Supporting Information, shows the same data as Figure 4, but it is divided between the different working buffers in order to show both ROH* and RO^-* on the same graph). It can be clearly seen in the figure that there is a major difference in the kinetic parameters between HPTS in bulk water and HPTS in the presence of insulin fibrils. Usually, the time-resolved emission decay of the ROH* form is composed of a rapid component (~100 ps), associated with the ESPT process and a slower component in the range of a few nanoseconds, which can be associated with the geminate recombination process.

In previous studies[18,29] reviewing the acid effect on reversible photoacids in aqueous bulk acidic solutions, it was found that the ESPT rate is unaffected up to about 1 M HCl. However, the amplitude of the long-time fluorescence tail of the time-resolved ROH signal increases as the acid concentration increases. This is clearly seen in Figure 4. The acid effect is attributed to the homogeneous protic reaction.

$$H_3O^+ + RO^-* \rightarrow ROH* \quad (2)$$

This reaction between the excess proton in solution with the RO^-* repopulates the ROH* that can undergo further photoprotolytic cycles.

Unlike the pH-dependent effect on the ROH* emission decay of HPTS in bulk water, it seems that the acidity of the solution does not affect the ESPT kinetic properties of HPTS when it is adsorbed on insulin fibrils (Figure 4a–c). The most obvious difference between the ROH* emission decay of HPTS in bulk water, in comparison to that with insulin fibrils, is the disappearance of the rapid proton-transfer rate, which becomes more than 10-fold slower (~1.2 ns). The slow rate of proton transfer of HPTS on the fibrils makes it hard to distinguish between what used to be a rapid rate of proton transfer to a slow geminate-recombination rate, which are both now on the same order of time scales.

A further indication of the slower proton-transfer rate of HPTS on insulin fibrils can be observed by following the rise-time of the fluorescence signal of the RO^-* form (Figure 4d,e). The rise-time of the RO^-* form is directly connected to the proton-transfer rate (Scheme 2); thus, unlike the ROH* emission decay, it should not be affected by a change in the pH, as can be observed in the image. Following the adsorption of HPTS on the insulin fibrils, the rise time of RO^-* increases from ~250 ps in bulk water to ~1 ns on the surface of fibrils.

HPTS on Cellulose. Unlike insulin amyloid fibrils, which are actually insoluble aggregates within the aqueous solution, cellulose can absorb water. When HPTS is adsorbed on dry cellulose (following evaporation of water from an HPTS–cellulose solution), the steady-state emission spectrum (black curve in Figure 5) consists of ~95% ROH emission and only ~5% of the RO^- emission. Since the sample was under ambient humid atmospheric conditions, some water molecules from the air are also adsorbed on the cellulose sample. We therefore assign the presence of the weak RO^- band at 520 nm to some inefficient and slow ESPT process that takes place in the (semi)dry cellulose.

Following the steady-state measurements of HPTS–cellulose in the dry state, we added, sequentially, 8, 15, and 30 μL of H_2O to the 15 mg sample of cellulose (corresponding to 53, 100, and 200% w/w of water). The spectra of the various samples consist of two emission bands, that of the protonated ROH band with a peak at ~448 nm and that of the deprotonated RO^- form with a peak at ~513 nm. It can be clearly seen that, as we add water to the dry cellulose (thus lowering its weight percentage), the intensity of the RO^- band increases, while that of the ROH band decreases, making it similar to the steady-state signal of HPTS in bulk water (green

dx.doi.org/10.1021/jp509153r | J. Phys. Chem. B 2014, 118, 13859–13869

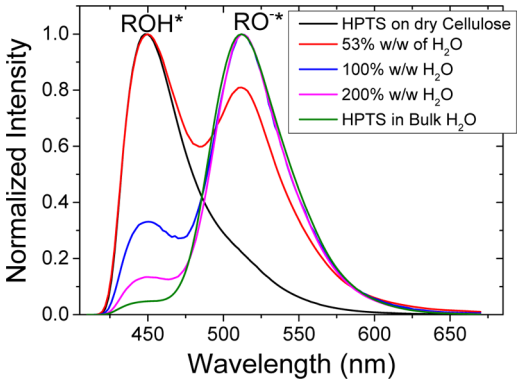

Figure 5. Normalized steady-state signals of HPTS adsorbed on dry cellulose and upon the addition of H_2O at several weight percentages, compared to HPTS in bulk H_2O.

curve). The photoprotolytic cycle starts with photoexcitation of the ROH form to the first electronic excited state, which then leads to an intermolecular proton-transfer reaction. The ROH hydroxyl proton is transferred to a nearby water molecule. The reaction rate constant in neat water is 10^{10} s^{-1}, and thus, the fluorescence decay time of the ROH form of HPTS is ~100 ps. We do not expect that an ESPT process can take place between the HPTS and the glucose units. In fact, HPTS in saturated water−sugar mixtures does not undergo an ESPT process.[30,31]

The radiative rates of the $S_1 \rightarrow S_0$ process for the protonated and deprotonated forms of HPTS are about the same, and the fluorescence lifetime in the absence of ESPT is about 5.4 ns. Proton geminate recombination (back to the ROH* form) takes place after the proton is transferred to the solvent. In neat water, the proton−RO^-* recombination is especially efficient for HPTS, since the RO^- anion of HPTS has four negative charges and the Coulomb attraction between the RO^- and the proton is large. The ROH* can undergo a second proton transfer, and the cycle can go on until the radiative rate depopulates both the ROH* and RO^-* forms. The geminate recombination contributes about half of the time-integrated fluorescence signal of the ROH form of HPTS. If the geminate-recombination signal is neglected, the proton-transfer rate constant k_{PT} can be evaluated from the band intensities of the steady-state spectra

$$k_{PT} = I_F^{RO^-}/I_F^{ROH}\cdot\tau_F^{-1} \quad (3)$$

where the radiative rate for HPTS is $\tau_F^{-1} = k_F = 0.19 \times 10^9$ s^{-1}. When the fluorescence band-intensity ratio $I_F^{RO-}/I_F^{ROH} = 10$, then $k_{PT} \approx 0.2 \times 10^{10}$ s^{-1} and $\tau_{PT} = 500$ ps. As mentioned above, geminate recombination in water contributes half of the steady-state ROH band intensity[24,25] and therefore the actual k_{PT} value in water is twice as great. In a condition of restricted water volume, as might be the case for HPTS in hydrated cellulose, geminate recombination might contribute even more to the ROH emission signal. As shown in Figure 5, the I_F^{RO-}/I_F^{ROH} ratio of the HPTS adsorbed on cellulose depends on the water content. For semidry samples (53% w/w of water, red curve), the ratio is rather small (0.7), whereas, for higher water content, the intensity ratios shown in the figure are 2.9 and 7.7 for 100 and 200% w/w, respectively. The results for the cellulose sample of high water content (200%, magenta curve) show that the proton-transfer rate for HPTS is about 3.5 times smaller than that of the bulk water sample for which the ratio is about 27.

Time-Resolved Emission. In order to complement the steady-state measurements and to employ the geminate-recombination rate (see the Theoretical Model section), we measured the time-resolved fluorescence of the ROH* and RO^-* forms of HPTS adsorbed on cellulose (Figure 6). When irradiated by UV light, cellulose shows broad emission in the

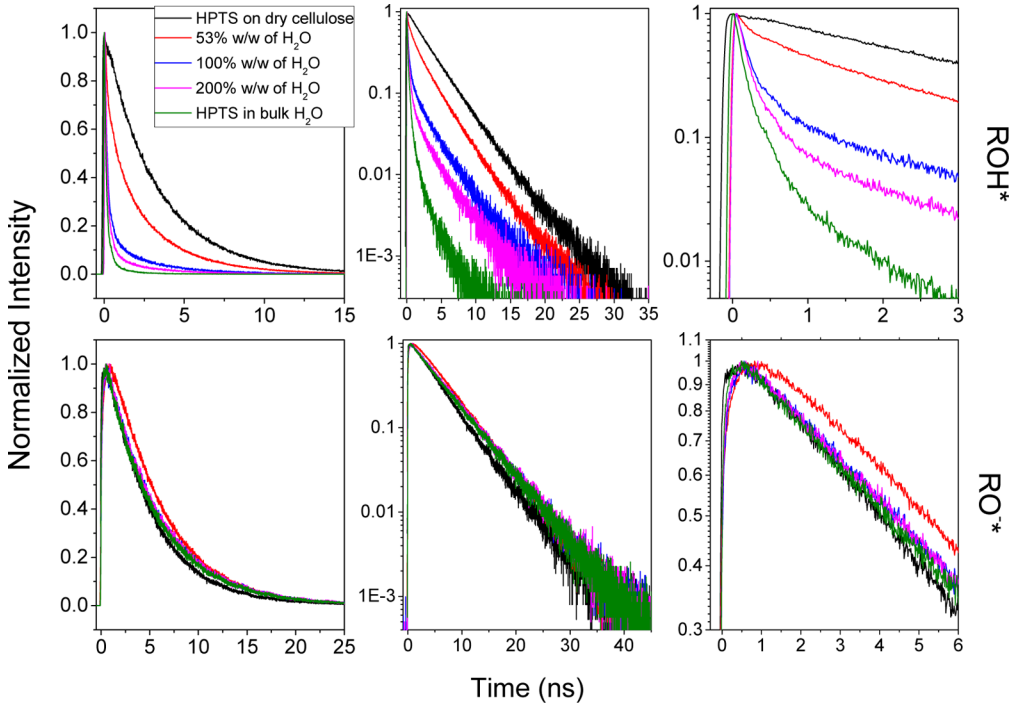

Figure 6. Time-resolved emission of HPTS adsorbed on cellulose at the detection wavelength of ROH* (440 nm) and RO^-* (535 nm), top and bottom graphs, respectively, in the dry state and for several weight percentages of H_2O added, compared to HPTS in bulk H_2O.

dx.doi.org/10.1021/jp509153r | J. Phys. Chem. B 2014, 118, 13859−13869

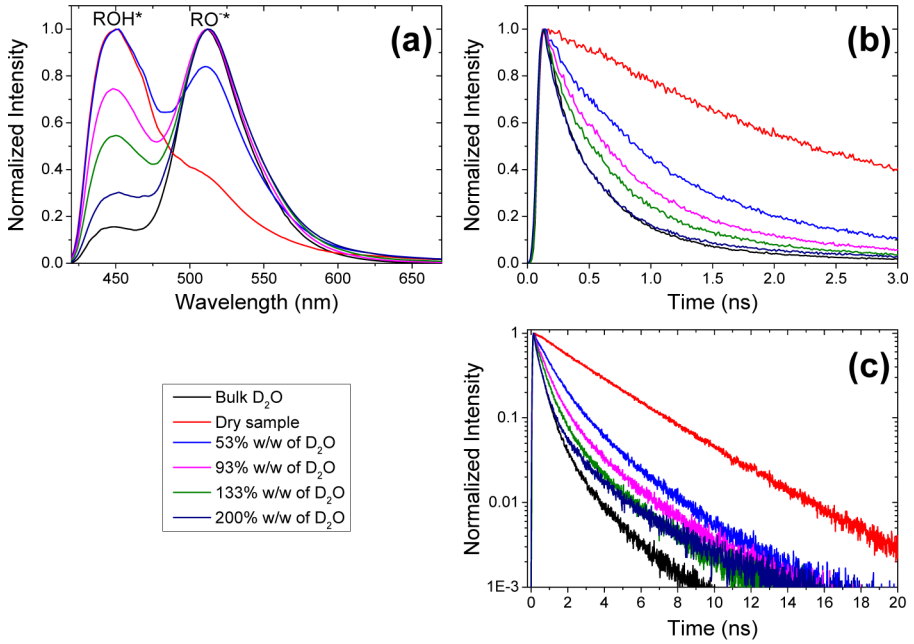

Figure 7. (a) Normalized steady-state and TCSPC signals (measured at 440 nm) shown on (b) normalized linear scale and (c) normalized semilog scale of HPTS adsorbed on cellulose in D_2O, compared to bulk D_2O measurements and dry-sample measurements.

Table 1. SSDP Fits to HPTS on Cellulose; Titration with H_2O

$W_{water}/W_{cellulose}$ (%)	k_{PT} (10^9 s^{-1})	k_a (10^9 Å·ns^{-1})	D (cm^2 s^{-1})	R_D (Å)	a_0 (Å)	dim.	τ_f^{-1} (10^9 s^{-1})
53	1.6	1.9	4.5×10^{-5}	28	6	*a*	0.18
100	6.5	3.7	7×10^{-5}	28	6	2.56	0.18
200	7.7	3.7	8×10^{-5}	28	6	2.5	0.16
bulk H_2O	9	7.3	9×10^{-5}	28	6	3	0.185

[a]The ESPT rate is small, and geminate recombination does not affect the ROH signal.

visible part of the optical spectrum. The fluorescence intensity of the cellulose is only $^1/_{40}$ of that of the HPTS (see Figure S2, Supporting Information). In the dry state, the emission decay time of the ROH* form is long (black curve, top panels) and almost independent of the monitored wavelength in the optical range of both bands, 440−520 nm (Figure S3, Supporting Information). When the amount of water is small (53% w/w of water), the fluorescence decay rate is rather small and the decay is nonexponential. We used simple data analysis to extract the rate of ESPT from HPTS to residual water in the dry sample on the basis of the following equation

$$k_F^{ROH} = k_{rad}^{ROH} + k_{PT} \quad (4)$$

where k_F^{ROH} is the fluorescence decay rate constant measured at 440 nm and k_{rad} is the radiative rate of ROH, which is about the same as that of the RO^- form, $(k_{rad}^{ROH})^{-1} \sim 5.0$ ns. The measured decay time at 440 nm is 3.8 ns, and k_F^{ROH} is 2.6×10^8 s^{-1}. Thus, the calculated proton-transfer rate constant of HPTS on dry cellulose is 0.6×10^8 s^{-1}.

As the water content is increased (to 100 and 200% w/w), the signal decay at short times (up to about 2 ns) is much larger. We assign the rapid decay-rate component to a high ESPT rate from an adsorbed HPTS molecule to a nearby pool of water. Protons in water exhibit a rather large diffusion constant. The exact structure of cellulose containing water is not known, though it is highly likely that some of the water molecules are tightly bound by the cellulose monomeric units. HPTS is a rather weak photoacid with $pK_{a,chem}^* = 0.7$.[18] In a previous study,[30,31] Gutman and co-workers found that the presence of sucrose in water lowers the ESPT rate.

Wet D_2O Cellulose−HPTS Samples. As discussed above, in the hydrated cellulose samples, the HPTS most probably goes into the aqueous phase of newly formed water pools. In order to verify this hypothesis, and to examine whether the aqueous phase inside the water pools has physical characteristics similar to those of bulk water, we measured the kinetic isotope effect (KIE). Figure 7 shows the normalized steady-state and time-resolved fluorescence (measured at 440 nm near the band peak of the ROH form) of HPTS on ∼15 mg of cellulose in the presence of 8, 14, 20, and 30 μL of D_2O, and the results obtained for bulk D_2O. As with the results obtained for water (Figure 5), the steady-state spectrum (Figure 7a) consists of two emission bands, those of the protonated (ROH) and deprotonated (RO^-) forms of HPTS, and the ratio of the band intensities I_{RO^-}/I_{ROH} varies with the D_2O content of the sample. These results indicate that the ESPT rate is high even when only 14 μL of D_2O is deposited on ∼15 mg of cellulose. Parts b and c of Figure 7 show on linear and semilogarithmic scales the time-resolved fluorescence of HPTS on ∼15 mg of cellulose in the presence of 8, 14, 20, and 30 μL of D_2O measured at 440 nm near the ROH-form band peak. As will be discussed below (in the Discussion section), the measured KIE indicates that the HPTS has indeed gone into the aqueous phase inside the water pools of the hydrated-cellulose samples.

Employing the Geminate Recombination Model. In the next section, we discuss the meaning of the fitting parameters of the photoprotolytic cycle of HPTS in both

dx.doi.org/10.1021/jp509153r | J. Phys. Chem. B 2014, 118, 13859−13869

Table 2. SSDP Fits to HPTS on Cellulose; Titration with D_2O

$W_{D_2O}/W_{cellulose}$ (%)	k_{PT} (10^9 s^{-1})	k_a (10^9 Å·ns^{-1})	D (cm^2 s^{-1})	R_D (Å)	a_0 (Å)	dim.	τ_f^{-1} (10^9 s^{-1})
53	1	0.9	3.5×10^{-5}	28	6	2.6	0.185
93	2.2	1.6	4×10^{-5}	28	6	2.6	0.185
133	2.4	1.7	4.2×10^{-5}	28	6	2.6	0.185
200	2.65	1.75	4.5×10^{-5}	28	6	2.6	0.185
bulk D_2O	2.85	2	6×10^{-5}	28	6	3	0.185

insulin and cellulose. We analyzed the time-resolved emission signals of the ROH form of HPTS in cellulose−water and cellulose−D_2O samples and also in bulk H_2O and D_2O by using the SSDP program of Krissinel and Agmon (Tables 1 and 2)[28] with a similar approach that had been previously used.[18,24,25]

The long time tail of HPTS on a cellulose−water mixture is composed of two contributions. The relative amplitude depends on the relative water content in the mixture. The first contribution arises from the proton geminate-recombination[24,25] with the RO^-* to reform the ROH* of HPTS molecules that desorb from the cellulose scaffold and enter the water pools. In bulk water, this fluorescence long-time tail decay law is given in eq 1. The second long-time fluorescence contribution probably arises from HPTS molecules that are adsorbed on the cellulose scaffold. The ESPT rate of this fraction of HPTS molecules is rather slow. We fit the time-resolved data of the ROH form of HPTS using the two components concept.

The ESPT rate of the slow component is about $k_{PT} \approx 0.3 \times 10^9$ s^{-1}. This rate is also the rate of the fluorescence decay of a "dry" cellulose sample under equilibrium with about 50% humidity of atmospheric air at 25 °C. The amplitude of this slow decay component decreases the larger the water content. At about 70% by weight water content, the amplitude of the slow component decreases to about 0.03 of the signal maximum.

We used the proton geminate recombination model[24,25] to analyze the HPTS time-resolved emission of the ROH signal. The decay begins from a large signal at short times, and the decay rate is determined mainly by the process of proton transfer to the solvent. At longer times, the geminate recombination repopulates the ROH form and the signal intensity approaches zero asymptotically at a much slower rate, as a power law ($t^{-\alpha}$). This property of the ROH signal decay enables us to obtain fine details with a background-free signal of the long-time ROH fluorescence decay, that is governed by the $H^+ \cdot\cdot RO^-$ geminate recombination. The tail amplitude of the ROH signal in bulk water at about 1 ns is only 0.04 of the initial signal intensity. In contrast to the ROH signal, the RO^- signal is almost unaffected by geminate recombination, which is superimposed on the strong radiative rate of RO^- and therefore it is almost unnoticed. The fit of the long-time tail of the ROH signal provides the proton diffusion constant D, as well as the diffusion space dimensionality, d.

For the cellulose samples, the slope is smaller and $\alpha = 3$ and the diffusion space dimension is a fractal of $d \approx 2.6$. This is explained by the nonspherical symmetry of the water pools formed in the cellulose water cavities, contained by the polymeric scaffold structure. If the water pools are elongated along the polymeric chain, the spherical symmetry breaks and the proton motion cannot be considered as obeying spherical symmetry, which is a prerequisite for a $t^{-3/2}$ power law.

The ESPT process mainly affects the initial decay rate, and thus, a good estimate of the rate constant is derived from the initial decay rate. The long-time decay and amplitude provide information on the parameters that determine the geminate recombination process. As seen from Tables 1 and 2, the ESPT rate depends rather weakly on the water content of the cellulose samples. The higher the water content, the higher the ESPT rate. The amplitude of the fluorescence tail is given by eq 1. There are many factors that are involved in the probability of the geminate recombination process. In the Discussion section, we provide a quantitative analysis and the values of the parameters and their dependence on the water content of the cellulose sample.

DISCUSSION

HPTS on Insulin Fibrils. The main finding obtained by following the photoprotolytic cycle of HPTS adsorbed on insulin fibrils is that the adsorption causes the ESPT rate from HPTS to water to decrease by about an order of magnitude, to about $k_{PT} \sim 10^9$ s^{-1}. From this, we learn that the surface of insulin fibrils is not accessible to bulk water molecules. Most probably, the highly negative HPTS molecule was adsorbed on one of the positively charged grooves along the cross-β structure of the insulin amyloid fibril (Figure 1). The second step of the photoprotolytic cycle (Scheme 2) is a proton geminate recombination process with RO^-*, the excited deprotonated form of HPTS. This process repopulates the ROH* form, and therefore, the time-resolved fluorescence decay signal shows a long-time fluorescence tail. As we showed in the previous section, the time dependence of the intensity and shape of this long-time fluorescence tail depends on the proton diffusion coefficient, D, and the proton diffusion space dimension, d. In bulk water, the ROH* fluorescence tail decays according to a power law ($t^{-d/2}$, and $d = 3$) for a three-dimensional diffusion space. We found that the fluorescence of the ROH* form of HPTS adsorbed on insulin fibrils decays as $t^{-\alpha}$, where α is closer to 1 (corresponds to a diffusion space dimension of 2) rather than 1.5 in unbound HPTS in bulk water. We explain this fractal dimension of ~2 by the breaking of the spherical symmetry of the ESPT process. The average diameter of the fiber is ~10 nm (perimeter of ~30 nm). The fluorescence lifetime of HPTS RO^-* is $\tau_F \approx 5.4$ ns, and the proton diffusion constant is known. Within the emission lifetime, the proton can reach, by diffusion, up to a distance of $L = (6D\tau_F)^{1/2}$ which is about 17 nm. Thus, the fibril diameter and the diffusion distance are of the same order and conditions of spherical symmetry do not hold. The shape of the proton-diffusion volume is close to that of a distorted hemisphere; thus, the proton diffusion is likely two-dimensional across the perimeter of the fibril, rather than a "standard" three-dimensional diffusion in bulk solution. The probability of proton recombination increases because of the fibril surface next to the HPTS molecule, and the effective dimension of the diffusion space decreases.

dx.doi.org/10.1021/jp509153r | J. Phys. Chem. B 2014, 118, 13859−13869

HPTS on Cellulose. The discussion on the interaction of HPTS with cellulose is more complicated. The interaction between microcrystalline cellulose and water has been studied by many techniques including sorption isotherms,[32−34] dielectric spectroscopy,[34] differential scanning calorimetry (DSC),[35] microcalorimetry,[16,36,37] and differential thermal and thermogravimetric analysis.[16] Fielden et al.[16] found that cellulose is a "molecular sponge" in the sense that the material is capable of physically retaining a high percentage of water within itself but allowing removal by evaporation to take place with great ease. This is observed by the freezing, melting, and evaporation phenomena observed in the DSC analysis. It shows that, at high water content, much of the water is free to solidify to ice on cooling and then melt and evaporate on heating. Agrawal et al.[15] studied the water distribution in cellulose by DSC where they found the presence of both freezing and nonfreezing water in hydrated cellulose. It was also observed that, for up to 18% w/w of water content in cellulose, there was no free water in hydrated samples, and all the moisture could be considered as tightly bound water. They also found that cellulose of 58% crystallinity can retain about 200% w/w water of which the major fraction is present as freezing water.

We found that the ESPT photoprotolytic cycle of HPTS on cellulose depends on the water adsorbed by the cellulose powder. When the water content is small, up to about three water molecules per glucose ring, HPTS is situated next to the cellulose scaffold and the nearest water molecules have the properties of "bound water". The ESPT rate at low water concentration is small and τ_{PT} is in the range of about 3−10 ns, of the order of the excited state lifetime of τ_F = 5.4 ns. When the water content adsorbed on cellulose is larger, the water tends to create "water pools" with free bulk-water properties. The affinity of HPTS to bulk water is larger than that for adsorption on the cellulose scaffold, since it is triply negative-charged. We therefore suggest that HPTS in water-rich cellulose mixtures is situated in the water pools rather than on the cellulose surface. The ESPT rate in large water pools is about the same as the value obtained in bulk water. The proton−RO^- geminate recombination rate in wet cellulose is greater than that in bulk water. The higher the water content, the lower the relative intensity of the geminate recombination fluorescence tail. The time-resolved fluorescence data of ROH in high-water-content cellulose could be nicely fitted by the SSDP program of Krissinel and Agmon.[28] The main difference between the ROH signals of HPTS in the different water/cellulose ratios and those in H_2O or D_2O is the intensity and shape of the long-time fluorescence tail. As discussed above, the decay of the fluorescence tail obeys a power law of $t^{-d/2}$, where d is the diffusion space dimension and this parameter is an important parameter in the fit of the intermediate and long-time tail. For HPTS adsorbed on cellulose, the value of d is smaller than that in bulk water or D_2O. We find that the best fit is for $d = 2.6 \pm 0.1$, which implies that the water molecules within the cellulose matrix are "frozen" in some small degree that slightly reduces the dimensionality of protons in the medium.

Our results on the ESPT from HPTS to water situated next to cellulose can be explained within the framework of previous findings by Fielden et al.[16] and Agrawal et al.[15] on the distribution of water within cellulose. We find in the current study that, for cellulose of low water content (less than ∼60% by weight), the average ESPT rate is rather low ($k_{PT} \leq 10^9$ s^{-1}), i.e., an order of magnitude smaller than in bulk water. We attribute the slow ESPT rate to the rather small water content and also to the ability of water to accept a proton from a photoacid. According to Fielden et al.[16] and Agrawal et al.,[15] the water in cellulose of low water content is tightly bound to the hydrophilic groups of cellulose. As we showed in a previous study,[27] tightly bound water molecules cannot participate in the ESPT process or solvate the hydronium ion that is formed in the process.

The ESPT rate also decreases when a photoacid is present in the aqueous phase of a reverse micelle of radius smaller than 15 Å.[38] It was found that the rate at which k_{PT} decreases in reverse micelles is rather slow. We found previously that the ESPT rate decreases exponentially with the thermodynamic activity of water (a_{water}).[27] In the current study, we find that, for a cellulose/water sample of low water fraction by weight, the rate of proton transfer is low, whereas, for samples of higher water content, the rate is close to that of bulk H_2O or D_2O. These findings are similar to the results obtained for a photoacid in a reverse micelle, for which the ESPT rate decreases only when the radius of the water pool is rather small and the radius of the water sphere is less than 15 Å.

The Kinetic Isotope Effect. The photophysics and photochemistry of excited molecules are complex, and the relaxation processes of the photoexcited molecule depend on the solvent and on the proximity to other media. The decay of the time-resolved emission of the ROH form provides the ESPT rate. Other relaxation phenomena such as solvation dynamics and nonradiative decay to other electronic states may be interfering with an unequivocal determination of whether an ESPT process is taking place. The kinetic isotope effect (KIE) is an excellent tool for determining that an ESPT process indeed takes place.

The ESPT process from a photoacid to water exhibits a fairly large KIE.[24,25,18,39,40] In general, the stronger the photoacid, the smaller the KIE; thus, for weak to mild photoacids of $pK_a^* > 0$ (like HPTS), the KIE is about 3, and for stronger photoacids of $pK_a^* < 0$, the KIE value is about 2.[41] Proton electrical conductivity shows a KIE of 1.45. This value is rather small and reflects the low barrier for proton transfer between two water molecules in bulk water. It also reflects the complexity of the proton-transfer reaction in bulk water.[18,42,43] In a more isolated system, such as the wild type green fluorescent protein (wt-GFP), the KIE is about ∼5.[44] This value may result from the fact that, in GFP, the proton-transfer system is less coupled to the environment and therefore the KIE is large.

In the current study, we have found that ESPT from HPTS to water next to a cellulose scaffold shows about the same KIE as that found for HPTS in bulk water, namely, KIE ∼ 3. The fact that we measured KIE values for the hydrated cellulose sample similar to that found in bulk water suggests that water pools exist in wet cellulose.

■ SUMMARY AND CONCLUSIONS

In the current work, we studied the excited-state proton-transfer (ESPT) process from an adsorbed photoacid on solid biomaterial to water molecules situated next to this biomaterial. We chose two biomaterials, hydrophobic insulin fibrils and hydrophilic cellulose powder, and employed steady-state and time-resolved optical techniques to measure the fluorescence of 8-hydroxypyrene-1,3,6-trisulfonate (HPTS), a commonly used photoacid. We found that the ESPT rate from HPTS to water adsorbed on insulin fibrils is lower by about an order of magnitude than that of bulk water ($k_{PT} = 10^9$ s^{-1} compared to

about 10^{10} s^{-1}). We also showed that the dimensionality of protons next to the surface of the fibrils is closer to 2, and not 3, as in bulk water. The second biomaterial on which we adsorbed the HPTS is cellulose. We showed that, when HPTS is adsorbed on a dry cellulose powder, ESPT does not take place. However, the ESPT process can be as efficient as in bulk water when the weight percentage is >100% $W_{water}/W_{cellulose}$. These ESPT findings on cellulose can be explained by the existence of several forms of water molecules in the sample.[15,16] Some of the water molecules are tightly bound by the cellulose scaffold, and cannot participate in the rapid ESPT, thus slowing the process nearly to the order of the radiative rate, ~5 ns. When the water content is high, most of the water molecules are not tightly bound and water pools are created. HPTS is triply negative charged, and it desorbs from the cellulose scaffold and resides in the water pools. Thus, the ESPT rate is about that measured in bulk water. The geminate recombination of the RO^- form of HPTS in water−cellulose samples shows a reduced dimensionality of about $d \approx 2.6$. We explain the lower dimensionality of the effective proton diffusion space by nonspherical symmetry of the effective diffusion space of the water pools formed next to the long polysaccharide chain of the cellulose.

Thus, in brief, we have shown that, by following the photoprotolytic cycle of HPTS, we can distinguish between the interaction of the photoacid with a hydrophobic biological surface that is less water-accessible (insulin fibrils) to hydrophilic biological matrixes that can absorb water (microcrystalline cellulose). By employing the geminate-recombination model, we could further follow the proton diffusion along the biological surface, where we found that the diffusion is not three-dimensional as in bulk water but has a reduced effective dimensionality. The diffusion of water molecules and hydronium ions (protons) in biological systems is one of the most important and fundamental process in nature. As for today, there is no easy experimental approach to follow this diffusion. The use of HPTS as a molecular fluorescent probe for following the interaction of a given surface or molecule with water molecules or protons is a straightforward approach, which can be easily employed for various biological, organic, or inorganic surfaces/molecules.

■ ASSOCIATED CONTENT

Supporting Information

(A) Time-resolved emission of HPTS in the working buffers of pH 1.6 and pH 6.6. (B) TCSPC background signals of cellulose. (C) TCSPC signals of HPTS adsorbed on cellulose. This material is available free of charge via the Internet at http://pubs.acs.org.

■ AUTHOR INFORMATION

Corresponding Author

*E-mail: dhuppert@post.tau.ac.il. Phone: 972-3-6407012. Fax: 972-3-6407491.

Notes

The authors declare no competing financial interest.

■ ACKNOWLEDGMENTS

This work was supported by grants from the James-Franck German-Israeli Program in Laser-Matter Interaction and by the Israel Science Foundation.

■ REFERENCES

(1) Jimenez, J. L.; Nettleton, E. J.; Bouchard, M.; Robinson, C. V.; Dobson, C. M.; Saibil, H. R. The Protofilament Structure of Insulin Amyloid Fibrils. *Proc. Natl. Acad. Sci. U. S. A.* **2002**, *99*, 9196−9201.
(2) Nelson, R.; Sawaya, M. R.; Balbirnie, M.; Madsen, A. Ø.; Riekel, C.; Grothe, R.; Eisenberg, D. Structure of the Cross-β Spine of Amyloid-Like Fibrils. *Nature* **2005**, *435*, 773−778.
(3) Hua, Q. X.; Weiss, M. A. Mechanism of Insulin Fibrillation: The Structure of Insulin Under Amyloidogenic Conditions Resembles a Protein-Folding Intermediate. *J. Biol. Chem.* **2004**, *279*, 21449−21460.
(4) Makin, O. S.; Serpell, L. C. Structures for Amyloid Fibrils. *FEBS J.* **2005**, *272*, 5950−5961.
(5) Tycko, R. Molecular Structure of Amyloid Fibrils: Insights from Solid-State NMR. *Q. Rev. Biophys.* **2006**, *39*, 1−55.
(6) Sievers, S. A.; Karanicolas, J.; Chang, H. W.; Zhao, A.; Jiang, L.; Zirafi, O.; Stevens, J. T.; Münch, J.; Baker, D.; Eisenberg, D. Structure-Based Design of Non-Natural Amino-Acid Inhibitors of Amyloid Fibril Formation. *Nature* **2011**, *475*, 96−100.
(7) Tycko, R. Solid-State NMR Studies of Amyloid Fibril Structure. *Annu. Rev. Phys. Chem.* **2011**, *62*, 279−299.
(8) LeVine, H., III [18] Quantification of β-Sheet Amyloid Fibril Structures with Thioflavin T. *Methods Enzymol.* **1999**, *309*, 274−284.
(9) Biancalana, M.; Koide, S. Molecular Mechanism of Thioflavin-T Binding to Amyloid Fibrils. *Biochim. Biophys. Acta, Proteins Proteomics* **2010**, *1804*, 1405−1412.
(10) Krebs, M. R.; Bromley, E. H.; Donald, A. M. The Binding of Thioflavin-T to Amyloid Fibrils: Localisation and Implications. *J. Struct. Biol.* **2005**, *149*, 30−37.
(11) Amdursky, N.; Erez, Y.; Huppert, D. Molecular Rotors: What Lies Behind the High Sensitivity of the Thioflavin-T Fluorescent Marker. *Acc. Chem. Res.* **2012**, *45*, 1548−1557.
(12) Crawford, R. L. In *Lignin biodegradation and transformation*; Wiley: New York, 1981.
(13) Updegraff, D. M. Semimicro Determination of Cellulose Inbiological Materials. *Anal. Biochem.* **1969**, *32*, 420−424.
(14) Klemm, D.; Heublein, B.; Fink, H.; Bohn, A. Cellulose: Fascinating Biopolymer and Sustainable Raw Material. *Angew. Chem., Int. Ed.* **2005**, *44*, 3358−3393.
(15) Agrawal, A. M.; Manek, R. V.; Kolling, W. M.; Neau, S. H. Water Distribution Studies within Microcrystalline Cellulose and Chitosan using Differential Scanning Calorimetry and Dynamic Vapor Sorption Analysis. *J. Pharm. Sci.* **2004**, *93*, 1766−1779.
(16) Fielden, K. E.; Newton, J. M.; O'Brien, P.; Rowe, R. C. Thermal studies on the interaction between water and microcrystalline cellulose. *J. Pharm. Pharmacol* **1988**, *40*, 674−678.
(17) Debye, P. Reaction Rates in Ionic Solutions. *Trans. Electrochem. Soc.* **1942**, *82*, 265−272.
(18) Agmon, N. Elementary Steps in Excited-State Proton Transfer. *J. Phys. Chem. A* **2005**, *109*, 13−35.
(19) Spry, D.; Goun, A.; Glusac, K.; Moilanen, D. E.; Fayer, M. Proton Transport and the Water Environment in Nafion Fuel Cell Membranes and AOT Reverse Micelles. *J. Am. Chem. Soc.* **2007**, *129*, 8122−8130.
(20) Tielrooij, K. J.; Cox, M. J.; Bakker, H. J. Effect of Confinement on Proton-Transfer Reactions in Water Nanopools. *ChemPhysChem* **2009**, *10*, 245−251.
(21) Amdursky, N.; Orbach, R.; Gazit, E.; Huppert, D. Probing the Inner Cavities of Hydrogels by Proton Diffusion. *J. Phys. Chem. C* **2009**, *113*, 19500−19505.
(22) Hutter, T.; Presiado, I.; Ruschin, S.; Huppert, D. Protic Properties of Water Confined in the Pores of Oxidized Porous Silicon Studied by Excited-State Proton Transfer from a Photoacid. *J. Phys. Chem. C* **2010**, *114*, 2341−2348.
(23) Soroka, H. P.; Simkovitch, R.; Kosloff, A.; Shomer, S.; Pevzner, A.; Tzang, O.; Tirosh, R.; Patolsky, F.; Huppert, D. Excited-State Proton Transfer and Proton Diffusion Near Hydrophilic Surfaces. *J. Phys. Chem. C* **2013**, *117*, 25786−25797.
(24) Pines, E.; Huppert, D.; Agmon, N. Geminate Recombination in excited-state proton-transfer Reactions: Numerical Solution of the

Debye−Smoluchowski Equation with Backreaction and Comparison with Experimental Results. *J. Chem. Phys.* **1988**, *88*, 5620−5630.
(25) Agmon, N.; Pines, E.; Huppert, D. Geminate Recombination in proton-transfer Reactions. II. Comparison of Diffusional and Kinetic Schemes. *J. Chem. Phys.* **1988**, *88*, 5631−5638.
(26) Collins, F. C.; Kimball, G. E. Diffusion-Controlled Reaction Rates. *J. Colloid Sci.* **1949**, *4*, 425−437.
(27) Huppert, D.; Kolodney, E.; Gutman, M.; Nachliel, E. Effect of Water Activity on the Rate of Proton Dissociation. *J. Am. Chem. Soc.* **1982**, *104*, 6949−6953.
(28) Krissinel, E. B.; Agmon, N. Spherical Symmetric Diffusion Problem. *J. Comput. Chem.* **1996**, *17*, 1085−1098.
(29) Solntsev, K. M.; Huppert, D.; Agmon, N. Challenge in Accurate Measurement of Fast Reversible Bimolecular Reaction. *J. Phys. Chem. A* **2001**, *105*, 5868−5876.
(30) Gutman, M.; Nachliel, E.; Kiryati, S. Dynamic Studies of Proton Diffusion in Mesoscopic Heterogeneous Matrix: I. Concentrated Solutions of Sucrose. *Biophys. J.* **1992**, *63*, 274−280.
(31) Gutman, M.; Nachliel, E.; Kiryati, S. Dynamic Studies of Proton Diffusion in Mesoscopic Heterogeneous Matrix: II. the Interbilayer Space between Phospholipid Membranes. *Biophys. J.* **1992**, *63*, 281−290.
(32) Zografi, G.; Kontny, M.; Yang, A.; Brenner, G. Surface Area and Water Vapor Sorption of Macrocrystalline Cellulose. *Int. J. Pharm.* **1984**, *18*, 99−116.
(33) Nakai, Y.; Fukuoka, E.; Nakajima, S.; Yamamoto, K. Crystallinity and Physical Characteristics of Microcrystalline Cellulose. *Chem. Pharm. Bull.* **1977**, *25*, 96−101.
(34) Khan, F.; Pilpel, N. An Investigation of Moisture Sorption in Microcrystalline Cellulose using Sorption Isotherms and Dielectric Response. *Powder Technol.* **1987**, *50*, 237−241.
(35) Khan, F.; Pilpel, N. The Effect of Particle Size and Moisture on the Tensile Strength of Microcrystalline Cellulose Powder. *Powder Technol.* **1986**, *48*, 145−150.
(36) Hollenbeck, R. G.; Peck, G. E.; Kildsig, D. O. Application of Immersional Calorimetry to Investigation of solid-liquid Interactions: Microcrystalline Cellulose-Water System. *J. Pharm. Sci.* **1978**, *67*, 1599−1606.
(37) Sadeghnejad, G.; York, P.; Stanley-Wood, N. Microcalorimetric Studies of Water Vapour Sorption in Macrocrystalline and Microfine Cellulose Powders. *J. Pharm. Pharmacol.* **1985**, *37*, 110P−110P.
(38) Cohen, B.; Huppert, D.; Solntsev, K. M.; Tsfadia, Y.; Nachliel, E.; Gutman, M. Excited State Proton Transfer in Reverse Micelles. *J. Am. Chem. Soc.* **2002**, *124*, 7539−7547.
(39) Bell, R. P. *The proton in chemistry*; Cornell University Press: Ithaca, NY, 1959; Vol. *1958*.
(40) Simkovitch, R.; Shomer, S.; Gepshtein, R.; Huppert, D. How Fast can a Proton-Transfer Reaction be Beyond the Solvent-Control Limit? *J. Phys. Chem. B* [Online early access]. DOI: 10.1021/jp506011e.
(41) Presiado, I.; Karton-Lifshin, N.; Erez, Y.; Gepshtein, R.; Shabat, D.; Huppert, D. Ultrafast Proton Transfer of Three Novel Quinone Cyanine Photoacids. *J. Phys. Chem. A* **2012**, *116*, 7353−7363.
(42) Geissler, P. L.; Dellago, C.; Chandler, D.; Hutter, J.; Parrinello, M. Autoionization in Liquid Water. *Science* **2001**, *291*, 2121−2124.
(43) Knight, C.; Voth, G. A. The Curious Case of the Hydrated Proton. *Acc. Chem. Res.* **2011**, *45*, 101−109.
(44) Chattoraj, M.; King, B. A.; Bublitz, G. U.; Boxer, S. G. Ultra-Fast Excited State Dynamics in Green Fluorescent Protein: Multiple States and Proton Transfer. *Proc. Natl. Acad. Sci. U. S. A.* **1996**, *93*, 8362−8367.